Defining Thalamic Nuclei and Topographic Connectivity Gradients ***in vivo***

Christian Lambert, Henry Simon, Jordan Colman, Thomas R. Barrick

PII: S1053-8119(16)30413-X
DOI: http://dx.doi.org/10.1016/j.neuroimage.2016.08.028
Reference: YNIMG13386

To appear in: *NeuroImage*

Received date: 19 March 2016
Revised date: 12 August 2016
Accepted date: 14 August 2016

Cite this article as: Christian Lambert, Henry Simon, Jordan Colman and Thoma R. Barrick, Defining Thalamic Nuclei and Topographic Connectivity Gradient ***in vivo***, *NeuroImage,* http://dx.doi.org/10.1016/j.neuroimage.2016.08.028

Defining Thalamic Nuclei and Topographic Connectivity Gradients *in vivo*

Christian Lambert*, Henry Simon, Jordan Colman, Thomas R. Barrick

Neurosciences Research Centre, Cardiac and Cell Sciences Research Institute, St George's University of London, United Kingdom.

***Corresponding Author:** Dr Christian Lambert, Neurosciences Research Centre, Cardiac and Cell Sciences Research Institute, St George's University of London, United Kingdom. clambert112358@gmail.com

ABSTRACT

The thalamus consists of multiple nuclei that have been previously defined by their chemoarchitectual and cytoarchitectual properties *ex vivo*. These form discrete, functionally specialized, territories with topographically arranged graduated patterns of connectivity. However, previous *in vivo* thalamic parcellation with MRI has been hindered by substantial inter-individual variability or discrepancies between MRI derived segmentations and histological sections.

Here, we use the Euclidean distance to characterize probabilistic tractography distributions derived from diffusion MRI. We generate 12 feature maps by performing voxel-wise parameterization of the distance histograms (6 feature maps) and the distribution of three-dimensional distance transition gradients generated by applying a Sobel kernel to the distance metrics. We use these 12 feature maps to delineate individual thalamic nuclei, then extract the tractography profiles for each and calculate the voxel-wise tractography gradients. Within each thalamic nucleus, the tractography gradients were topographically arranged as distinct non-overlapping cortical networks with transitory overlapping mid-zones.

This work significantly advances quantitative segmentation of the thalamus *in vivo* using 3T MRI. At an individual subject level, the thalamic segmentations consistently achieve a close relationship with *a priori* histological atlas information, and resolve *in vivo* topographic gradients within each thalamic nucleus for the first time. Additionally, these techniques allow individual thalamic nuclei to be closely aligned across large populations

and generate measures of inter-individual variability that can be used to study both basic function and pathological processes *in vivo.*

KEYWORDS

Thalamus; Segmentation; Tractography; Diffusion Weighted Imaging; Spiral loops; Connectivity

INTRODUCTION

The thalamus is a paired diencephalic structure consisting of multiple nuclei. These underpin a broad array of functions via densely interconnected reciprocal connections between the cortex, basal ganglia, cerebellum, brainstem and spinal cord[1]. The thalamus primarily controls information passing to and from the cerebral cortex by relaying primary sensory inputs, gating descending cortical outputs, integrating information across networks and modulating cortical laminar synaptic activity via reciprocal cortico-thalamic-cortico connections[2].

Thalamic nuclei have previously been delineated on an *ex vivo* basis, exploiting the differing chemoarchitectual and cytoarchitectual properties of the various cellular populations to identify unique, functionally specialized territories[3]. Whilst several parcellation schemes exist, Morel's[3] is widely accepted and divides the thalamus into five broad groups: Anterior, Posterior, Medial, Lateral and Reticular. These groups can be further separated into 30 nuclei based upon cytochemical staining properties (Fig. 1).

Whilst the action of the thalamus has been extensively studied, there still remain many fundamental questions surrounding the composite microcircuits underpinning basic brain functions[5]. Additionally, there are several neurodegenerative diseases where selective patterns of pathological involvement are seen in the thalamic nuclei, such as the mediodorsal nuclei in Parkinson's disease[6], the anterio-dorsal nucleus in Alzheimer's disease[7] or the anterior nuclear group in prion disorders[8]. Beyond these structural abnormalities, abnormal firing patterns in thalamic neurons have been observed across a

broad range of conditions including epilepsy, psychosis, and obsessive-compulsive disorders[2]. In functional neurosurgery, the targeting of distinct thalamic targets using deep brain stimulation has been successfully used to treat several conditions including tremor, chronic pain and epilepsy.

Diffusion-weighted imaging (DWI) is a non-invasive modality that uses magnetic resonance imaging (MRI) to measure the bulk diffusive motion of protons *in vivo*[9], and reflects the underlying tissue microstructure. Using DWI, the spatial distributions of white matter fibers can be estimated for a single voxel via a technique known as probabilistic tractography[10]. These estimated white matter pathways have been shown to correspond with the histological anatomy[11], and have been widely used to delineate regions that are not visible using conventional MRI techniques[12]. Consequently, there have been a number of previous attempts to delineate the internal structure of the thalamus *in vivo* using DWI and probabilistic tractography. The majority of these have utilized top-down clustering techniques to varying degrees[13-16,52,53], employing a categorical *a priori* parcellation to cluster thalamic voxels according to metrics based on connectivity strength[13,14], probability[15], principal diffusion direction[16] or a mixture of these metrics[53]. However the main limitation with these approaches is the parcellation of the brain into categorical units based on gross anatomy. It is known that the underlying cytoarchitecture *in vivo* exhibits large variability both across subjects as well as between hemispheres, which do not precisely map to visible gyral contours[17].

This work was motivated not only by the recognized limitations and problems in tractography-based segmentation outlined above, but also by the problem of accurately defining and representing anatomical boundaries[47]. Specifically, both graduated and abrupt transition zones are known to exist between anatomical regions, and these can be observed in both cortical[19] and subcortical structures[1,51]. This variability in boundaries has clear methodological implications, as the widely used hard-clustering methods for brain parcellation[59-61] will be unable to accurately model or demonstrate graduated architectural features and instead will artificially provide "*anatomically distinct boundaries*" as necessary methodological by-products[62-64].

Here we provide a more biophysically realistic segmentation and representation of the thalamus, allowing inter-individual variability to be more accurately quantified and improve alignment of homologous thalamic nuclei for voxel-wise analysis, allowing both basic function and pathophysiological processes to be better studied *in vivo*. Based on an *ex vivo* technique for delineating cytoarchitectual regions[19] , we developed a stable and anatomically congruent technique using DWI data acquired from the Human Connectome Project. We reliably delineate nine thalamic nuclei at an individual subject level *in vivo*, using probabilistic tractography data in a fully automated bottom-up fashion, and demonstrate good correspondence to histological anatomy. We provide a comprehensive description of the connectivity profiles for each nucleus, and relate them to their proposed functions. Furthermore, we define transitory topographic tractography gradients within each nucleus and demonstrate how this ordered internal sub-structure relates to patterns of whole brain connectivity. Finally, we examine the overlap between these tractography gradients, and find evidence for topographically arranged overlapping and non-overlapping white matter networks.

METHODS

Technical Definitions

These are described more fully within the methods, but are provided for clarity:

- *Feature Map:* Six summary parameters for voxel-wise distributions - Mean amplitude, mean, variance, skewness, kurtosis and the median.
- *Transition Gradient:* The value of the 3D Sobel kernel applied to the local Euclidean Distance (ED) values.
- *Transition Gradient Feature Map:* A distribution of transition gradient values generated by applying the 3D Sobel kernel to each of the 26 connected neighbors, summarized as feature maps.
- *Topographic Tractography Gradient:* The primary eigenvector value generated by eigendecomposing a sub-ED matrix corresponding to a thalamic nucleus.

- *Gradient Overlap:* Defined by examining the overlap of whole brain tractography distributions that correspond to the voxel specific topographic tractography gradient values.

Data acquisition

40 subjects (19 male) from the minimally processed Q2 Human Connectome Project (HCP) data release was used in this study. The isotropic high-resolution (0.7 × 0.7 × 0.7 mm) T1-weighted (T1w), Freesurfer cortical parcellation and high angular resolution diffusion images (1.25 × 1.25 × 1.25 mm) were extracted for each subject. Acquisition protocols, and pre-processing steps are described elsewhere[20].

Data preprocessing - Diffusion

Using the FSL software v5.0 (http://fsl.fmrib.ox.ac.uk/fsl/fslwiki/), tensor estimation was performed using DTIfit. Following this, voxel-wise estimation of fiber orientation distribution was undertaken using the GPU enabled multishell model of bedpostX[21], estimating three fibers per voxel.

Data preprocessing - HCP Structural

T1w images were segmented in SPM12[22] into three tissue classes; grey matter (GM), white matter (WM), cerebrospinal fluid (CSF). These high-resolution segmentations were warped to a population-specific group average template using the diffeomorphic warping "*Shoot*" algorithm in SPM12[23]. The native T1w images were also skull-stripped by masking with a sum of all three segmentations at a threshold of 0.1. The skull stripped T1w images were inverted (1/T1w) because the non-linear warping algorithm in FSL (FNIRT) uses the sum of square differences as its cost function, which is more sensitive to differences in contrast compared to mutual information or cross correlation[54]. These were used to estimate 5mm isotropic deformation fields to the diffusion FA images using FNIRT in FSL.

For each individual, the Freesurfer thalamic parcellation was extracted and projected onto the high-resolution T1w images and manually refined using ITK-SNAP[24]. The following

boundaries were used: Laterally, the posterior limb of the internal capsule; Medially the lateral walls of the third ventricle; Anteriorly, the interventricular foramen and head of the caudate nucleus; Posteriorly the splenium of the corpus callosum, lateral ventricle, and fornix; Superiorly, the thalamus is enclosed by the fornix and lateral ventricle; Inferiorly, the hypothalamus (defined using the hypothalamic sulcus), tegmentum and superior colliculus. Particular care was taken to ensure any voxels within the fornix or ventricles were fully removed.

The FNIRT derived deformation fields were used to warp the T1w defined grey, white and CSF segmentations, refined thalamus ROIs, Freesurfer cortical parcellation and T1w image into diffusion space. The GM, WM and CSF segmentations in diffusion space were also warped to a group average template using the diffeomorphic warping "*Shoot*" algorithm in SPM12[23].

Probabilistic Tractography

For each individual, every voxel in the thalamic ROI was used as a seed for probabilistic tractography using probtrackX in FSL. The left and right thalamus was considered independently. The CSF segmentation was binarised at a threshold of 0.2, and used as an exclusion mask to avoid any erroneous tracking into the ventricles or outside the brain. Each voxel was sampled 5,000 times using the proportional sampling option with three fiber distributions, a curvature threshold of 0.2 and loop-check on. The *–omatrix2* option was used as the output, creating a sparse connectivity matrix containing the probabilistic index of connectivity (PICo) from each thalamic ROI voxel to every other brain voxel. PICo is defined as the proportion of the total number of samples from a seed voxel that reach a target area, and ranged from 0 to 5000 in the native connectivity matrix.

Thalamic Tractography Segmentation

Fig. 2 summarizes the steps described. For this step, no thresholding was applied at any stage:

1. For each individual thalamus (M seed voxels), the voxel-wise tractography distributions were input to a large sparse connectivity matrix (M×N, where N is the total number of brain voxels).

2. Using the whole-brain tractography data, a M×M correlation matrix was calculated. The Euclidean Distance (ED) between each of the entries in the correlation matrix was calculated, and used to construct a M×M ED matrix. The Euclidean distance provides pair-wise measures of similarity between all of the tractography distributions for the entire thalamus. The more dissimilar the distributions, the higher the distance values.

3. For each individual voxel, the corresponding ED distribution was treated as a frequency curve to calculate six new feature maps. The six features were based upon the *ex vivo* observer independent cytoarchitectual delineation approach[19], and were the mean amplitude, the first four central moments about the mean (mean, variance, skewness and kurtosis) and the median.

4. The Sobel kernel is a well-defined simple method of edge detection that can be applied in three dimensions to define gradients within images[25]. At each seed voxel, a 3D Sobel kernel (3 × 3 × 3) was applied using the 26 connected neighbors, providing measure of the transition gradient strength between the ED vectors for each voxel.

5. The 3D Sobel kernel was then centered on each of the connected neighbors and the process repeated, providing a histogram of gradients for the seed voxel and 26 connected neighbors. These histograms were summarized using the same features as previously described in step 3, and the process repeated across all seeds providing six further voxel-wise feature maps for the transition gradients. These twelve feature maps allowed individual voxels to be characterized based on their tractographic properties rather than connectivity profiles, and do not rely on any user defined *a priori* assumptions such as thresholding the distributions or parsing them into cortical regions of interest based on secondary connectivity metrics.

6a. The next objective was to use the feature maps to achieve parcellation of the thalamic nuclei. All the feature maps (F = 12) for every individual (P = 40) were first constrained by a bounding box (image dimensions: $D_1 = 56$, $D_2 = 51$, $D_3 = 26$) to increase processing speed and reduce physical storage and normalized by each images maximum value so all values ranged between 0 and 1 (the skewness maps were first shifted by the minimum voxel value prior to normalizing so all values were positive). The left and right normalized maps were joined before warping to a group-average diffusion space using the deformations toolbox in SPM12 and the *Shoot* calculated warp fields.

6b. In group-average space, each warped normalized feature map was input to a sparse 5D matrix ($D_1 \times D_2 \times D_3 \times F \times P$). A modified multivariate Mixture of Gaussians (mmMoG) was used to cluster the entire dataset and generate tissue probability maps (TPMs) as previously described in Lambert et al., 2013[26]. Each cycle was iterated 100 times. Because we had no *a priori* regarding optimal cluster number, we performed clustering from 4 to 32 clusters in steps of 2, and took the final log-likelihood from mmMoG to calculate the Bayesian Information Critereon (BIC). This indicated the optimal solution (i.e. BIC minima) was provided by 22 clusters (Fig. 2). The whole process was repeated three times to ensure consistent solutions and avoid local minima, and the same result was achieved.

6c. Inspecting the initial 22 TPMs, there were 9 intra-thalamic maps, one for the midline intra-thalamic adhesion and one non-thalamus. The remaining 11 TPMs represented edge and partial volume voxels, and were concatenated into a single TPM for ease of use. This provided a final total of 12 new tissue classes.

7. The new TPM were used to replace the default SPM12 TPMs. The default segment parameters were changed to use six Gaussians per TPM, with bias correction and regularization turned off, and modified to utilize the calculated warps between group average and individual thalamic space.

8. Each joint feature map (F=12) was used as a separate channel in the segmentation pipeline. This was then used to segment the thalamus over the entire population. This achieves thalamic segmentation at the individual single subject level by using the well established "Unified Segmentation" approach[22] that combines the voxel intensities (12 native feature maps in this case) and spatial priors (back projected TPMs) in a probabilistic approach. The added advantage with this approach is that the pre-calculated TPMs can be used directly in SPM to allow step 6 to be bypassed, and hence the technique may be easily applied to future datasets of lower resolution and quality in a way similar to the current SPM segment with T1w images. The 10 thalamic segmentations in native space (9 intrathalamic, 1 intrathalamic adhesion), were used to calculate a new thalamic group average template, again using the "*Shoot*" algorithm in SPM12. All native segmentations were warped to the thalamic average space to create a group average image, and calculate voxel overlap.

9. The tractography thalamic segmentation approach defined above allows structurally homogenous sub-regions (i.e. nuclei) to be identified that exhibit smooth changes in their ED-transition gradient profiles. To define the topographic tractography gradients within the anatomical connectivity of these sub-regions, the corresponding ED values were extracted from the M×M matrix, and eigendecomposed. The principal eigenvector was extracted and the components projected back to each voxel within the individual subject space. For each nucleus, these topographic tractography gradients maps were warped to group average thalamic space to create average maps.

Defining Segmented Nuclear Groups

The thalamic nuclei were labeled according to the closest matching nuclei from Morel's Atlas. To verify the nuclear allocations, the mean three-dimensional atlas of the human thalamus[5] generated from Morel's histological data by Krauth et al[55] was used (licensed from University of Zurich and ETH Zurich; © University of Zurich and ETH Zurich, Axel Krauth, Rémi Blanc, Alejandra Poveda, Daniel Jeanmonod, Anne Morel, Gábor Székely). This supplies segmentations for the 30 nuclei shown in Fig. 1 as surface images

in legacy .vtk file format. In order to use these with our MRI data, the a polygon mesh voxelisation algorithm obtained from MATLAB central was used (available at http://www.mathworks.com/matlabcentral/fileexchange/27390-mesh-voxelisation). The MATLAB code was modified to allow multiple polygons to be simultaneously processed into a single three-dimensional matrix, and output as a nifti file with each nucleus allocated to a separate label. This thalamic atlas ROI was then manually scaled and aligned as closely as possible to the group average thalamus using spm_check_registration. Using the group average overlap maps, the percentage volume of each atlas thalamic nucleus occupied by our segmentations was calculated, where each atlas voxel was allocated to the most likely segmented class (i.e. highest probability in group average space), thereby ensuring a maximum of 100%. These results are provided in full in Supplementary Figure 2 and Supplementary Table 1.

Topographic Tractography Gradient Analysis

For each seed voxel within each thalamic cluster the corresponding tractography distribution was extracted and PICo values less than 10 were set to zero. For every brain voxel containing a tract, the thalamic nucleus seed voxel with the highest PICo value was identified, and the corresponding eigenvector value ("*topographic tractography gradient*") was mapped to that brain voxel. In this way, topographic graduated patterns of connectivity could be calculated for each individual across the population. These maps were warped to group average space to create averaged topographic tractography gradients for each thalamic nucleus.

Finally, to assess the overlap between tractography distributions within each thalamic nucleus, the total range of topographic tractography gradient values were initially divided into quintiles. The tractography distributions representing the lower, middle and upper quintiles were selected for further analysis. These were used to create three corresponding tractography maps (lower, middle and upper quintiles). These maps were masked to include only voxels that were located within the cortical and subcortical Freesurfer ROIs, and used to calculate the percentage overlap in the tractography distributions between the gradient quintiles for each nucleus.

Connectivity Strength

For each thalamic cluster, the sparse whole brain connectivity matrix was taken. All PICo values less than 10 were zeroed, but the matrix was not binarised. Overall, the objective was to assess the strength of connectivity within each thalamic nucleus, to every other parcellated brain region generated by Freesurfer (43 regions of interest from the aparc+aseg images supplied as part of the minimally processed HCP data set: 35 cortical and 5 subcortical for each hemisphere, plus the whole cerebellum, brainstem and ventral mesencephalon). Both the target ROI volume and distance from the seed voxel confound connectivity metrics generated from the PICo values, and so to mitigate for these effects the "*Normalised Connectivity Strength*" (NCS) was generated:

$$NCS_j = \frac{\sum_{i=1}^{k} PICo_{ROI_j}}{\left(\sum_{j=1}^{Z=43}\sum_{i=1}^{k} PICo_{ROI_j}\right) \times Volume\ ROI_j}$$

Where *k* is the total number of voxels within the *jth* Freesurfer ROI. For each of the nine nuclei, a matrix of normalized connectivity strengths between all Freesurfer ROIs (1 × 43) was generated for every individual, taking the mean value between the two hemispheres. To better visualize the patterns of connectivity, the subcortical and cortical ROIs were visualized separately.

Overlap Analysis

To assess the stability and consistency between the segmentations over the whole group, each subject's segmentations were binarised at a threshold of 0.2 and warped to group average space using nearest neighbour interpolation. For each thalamic nucleus, an average image (*"thalamic nucleus overlap map"*) was created to assess the spatial stability of the segmentations. Additionally, we calculated the threshold-overlap ratio, defined as the sum of all voxels binarised at a set threshold between zero and one, divided by the sum of all binarised voxels greater than zero, for each group average thalamic nucleus across a range of thresholds (1000 steps between 0.01% and 100%

group average overlap). We repeated this process with the Oxford thalamic connectivity atlas[18] for comparison.

RESULTS

Feature Maps

The group average feature maps are shown in Fig. 3. Note that these are not patterns of connectivity, but instead represent the type of spatial distribution exhibited by white matter tracts within each voxel, compared to all other thalamic voxels. These demonstrate a well-ordered structure with distinctive regions of the thalamus exhibiting similar tractographic properties and displaying clear transition boundaries.

Tractography Parcellation

The thalamus was parcellated into nine nuclei (Fig. 4 and Supplementary Fig. 1). The feature map properties of these nuclei are also summarized in Fig. 5. The thalamic nuclei identified were labeled according to the closest matching nuclei from Morel's Atlas[3]: Anterior (ANT), posterior-anterior (pANT), mediodorsal (MD), intralaminar midline group (IL), vertroanterior (VA), ventrolateral (VL), ventroposterior (VP), pulvinar (PUL) and geniculate (GEN) groups. These were verified by quantifying the overlap with the 3D thalamic histological altlas[55] (Supplementary Fig. 2; Supplementary Table 1). Of these, the ANT, MD, VL, and VP corresponded closely with the atlas, with >80% overlap compared to the histological data (Supplementary Fig. 2). The GEN and PUL corresponded extremely well with the posterior group, but contained a mixture of the nuclei within this (Supplementary Table 1). Partly, this is due to the differences in how the atlases are generated and alignment difficulties in this posterior section (Supplementary Fig. 2c). The IL group matched reasonably well, but in a minority of subjects also included areas more posteriorly (Fig. 7), and consequently contained a broader a mixture of nuclei. Two segmentations clearly contained more than one identifiable nucleus. First, the VA group that formed a curved structure (Supplementary Fig. 1), fusing with the ipsilateral hypothalamus. Based on the histological 3D atlas, a significant portion of this appears to be the centre médian and central lateral nucleus that

surrounds the mediodorsal nucleus (combined overlap >50%), but may also contain adjacent pathways such as the mamillothalamic tract (MTT)[27] or hypothalamic-thalamic pathways. A region in the posterior thalamus was also included in VA that may represent part of the internal medullary laminar, which is also closely associated with VA and MTT. Second, the pANT group contained lateral-posterior nuclei (30% overlap), medial pulvinar (19% overlap) and posterior portion of the central lateral nucleus (40% overlap). This again may be a consequence of their vicinity to the internal medullary laminar and also their similar connectivity profiles. These discrepancies emerge because the thalamic parcellations described here are based entirely on myloarchitectual properties rather than histological cytoarchitectural features[3]. Despite the fundamentally different approaches between our approach and *ex vivo* mapping methods (i.e. *in vivo* tractography based on MRI derived measures of brain diffusion versus *ex vivo* histological cell staining that is largely based on calcium binding proteins), operating at completely different length scales (>1mm versus <10μm), there remains a high degree of overlap and agreement with *ex vivo* histology (Fig. 8, Supplementary Fig. 2).

Thalamic nuclei connectivity and topographic Gradients

Each nuclear group was characterized according to the connectivity strength to a Freesurfer parcellated brain (detailed in the methods). The sub-cortical and cortical regions of interest (ROIs) were analysed separately, as the marked differences in their proximity would skew measures of connection strength. The normalised connectivity strength of each thalamic nucleus to a parcellated ROI is provided in Fig. 5 and summarized in Supplementary Table 2. For each nucleus, the topographic gradient in connectivity was defined and the transitions in connectivity patterns explored (Fig. 6). For clarity, each voxel within the tractography results shown in Fig. 6 has the gradient value of the corresponding seed with the strongest connectivity (i.e. winner takes all) over the entire structure.

A. Anterior Group

These displayed strongest connectivity to the frontal pole, orbitofrontal cortex, insula, precuneus and supramarginal gyrus. Subcortically, there was strong connectivity to the striatum, amygdala and hippocampus, in keeping with its known direct connectivity via the fornix, underpinning different aspects of episodic memory[8]. The connectivity gradient was arranged along the anterio-posterior axis, with the anterio-medial portions of the nucleus projecting more to the prefrontal cortex, medial temporal lobe and ventral tegmental area[8], whereas the posterior-lateral aspect, encompassing the anterio-ventral and anterio-dorsal nuclei, had stronger projections to the superior-lateral frontal cortex, retrosplenial cortex and the brainstem. Experimental studies have demonstrated that these posterior-lateral anterior nuclei are involved in head direction and spatial navigation[8], with direct connections to the brainstem[28], frontal eye fields[29], secondary motor cortices and retrosplenial cortex[8].

B. Posterio-Anterior Group

This group predominately consists of the lateral-posterior (LP) nucleus and medial pulvinar. There was strong cortical connectivity to the precuneus, superior parietal & frontal gyrii, and primary sensory-motor cortex, and subcortically to the caudate, pallidum and brainstem. These formed a lateral to medial orientated gradient of connectivity. Laterally, there was greater connectivity to the primary sensory-motor cortices, posterior pallidum, posterior cingulate, dorsal brainstem and cerebellum. Medially the projections were to the occipital cortex, parietal cortex, medial temporal lobe, superior-lateral frontal cortex and anterior cingulate. This nuclear group is divided into dorsal and medial groups, with the latter merging with the pulvinar. The connectivity supports the lateral nucleus as an analogue of the dorsal division of LP. These are known to have dense, topographically arranged connections with the cerebellum and dorsal columns[30], in addition to the parietal cortex[31], and are involved in visual attention and spatial integration cortical networks[32].

C. Mediodorsal Group

Cortically the superior, middle and inferior frontal gyri and temporal pole displayed the strongest connectivity overall, but also the cingulate gyrus had relatively high levels of

connectivity compared to other nuclei. Subcortically there were high levels of connectivity to the basal ganglia complex. There was a clear transition in the connectivity gradient between the anterior region with projections to the pre-frontal regions, and the posterior region with projections to the pre-motor and supplementary motor cortices, in agreement with animal literature[33]. Functionally, MD is mainly involved in maintaining and modulating working memory[34] and has been proposed to have three principal subdivisions: medial, central and lateral[35] that exhibit topographic projections to the frontal lobe and cingulate cortex[36]. The medial division particularly is more densely connected with the medial temporal lobes and ventral tegmental area[35], whereas the posterior portion receives highly convergent pathways from the motor regions[33] and pallidum[35], all of which are observed in our data (Fig. 6c).

D. Intralaminar Group

The midline IL group displayed a broad pattern of connectivity to the orbitofrontal, enterorhinal and calcarine cortices, and subcortically to the striatum, amygdala and ventral mescencephalon. Partly, this maybe a consequence of the higher levels of variability in this nucleus (Fig. 7 and 8, Supplementary Fig. 2), leading to a less well defined topographic tractography gradient compared to other nuclei, that is arranged along a superior-anterior to inferio-posterior axis. Cortically, these tracts overlapped with each other, however the anterio-superior portions did display more selective connectivity to the hypothalamus, brainstem and medial temporal lobe. These nuclei are known to receive extensive inputs from the upper brainstem neuromodulatory nuclei[37], reciprocally connect the medial temporal lobe and prefrontal cortex[38] and are proposed to modulate memory networks.

E. Ventroanterior Group

Whilst the posterior aspect of this group contributed to more variability in group-average overlaps, the anterior cluster (VA proper) was highly stable (Fig. 7 and 8). Overall, high levels of connectivity were observed in the frontal cortices, temporal pole, pericalcarine gyri, basal ganglia, amygdala and ventral mescencephalon. The gradient analysis clearly separated the anterior VA cluster from the more variable posterior cluster. Anteriorly, the

projections were to the hippocampus, prefrontal cortex and mesencephalic structures (VTA and raphe anteriorly, substantia nigra more posteriorly). The posterior group projected to the visual and motor corticies, reflecting their location within the pulvinar complex. Previous studies have shown the VA nucleus receives dense projections from the globus pallidus[39] and substantia nigra, and projects extensively to the frontal lobe[40], anterior cingulate[41] and intrathalamically to the IL and MD groups[40]. The function of VA is ill defined but is thought to modulate basal-ganglia motor activity[32] and speech[42].

F. Ventrolateral Group

This group had high levels of cortical connectivity to the primary motor cortex, superior and middle frontal gyri and frontal pole, and subcortically to the striatum and brainstem. The gradient of connectivity was aligned along an anterior-rostral to posterior-caudal axis. The posterior aspect had greater connectivity to the motor-sensory cortices, mesencephalon, bilateral cerebellum and brainstem. Anteriorly, VL had greater connectivity to prefrontal regions including the inferior frontal gyri (motor speech areas), with some connectivity to the medial temporal lobe. The posterior VL thalamus forms a major relay circuit between the motor cortex and cerebellum, whereas lesions situated within the anterio-medial portions of VL cause abnormalities in verbal fluency and speech[32].

G. Ventroposterior Group

This group exhibited strong connectivity to both the primary motor and sensory cortices, in addition to the superior frontal gyrus, insula and brainstem. The gradient was similarly orientated to the VL thalamus along an anterior-rostral to posterior-caudal axis. This group represents the major sensory nuclei of the thalamus[13] with extensive topographically arranged connections to the primary and secondary sensory cortices, vestibular nuclei and pre-motor cortices[43].

G. Pulvinar Group

The pulvinar forms a large complex in the dorsal thalamus with at least four internal subdivisions[44] involved in visual procession and multimodal sensory integration[32]. We

found high levels of connectivity with the primary motor-sensory cortices, superior parietal gyrus, precuneus and visual cortex. The connectivity gradient aligned along an anterior–posterior axis. The posterior aspect projected to the primary visual cortices, temporal lobe and pre-frontal regions, suggesting it contained the inferior and medial pulvinar nuclear groups. In contrast, the anterior gradients projected to the primary motor-sensory cortices, parietal cortex and brainstem. These are more consistent with the anterior and lateral pulvinar subdivisions that contribute to the integration of somatosensory and visual information[32].

I. Geniculate Group

These had strong connections with the primary visual areas, temporal pole and brainstem. The connectivity gradients clearly separated into medial and lateral structures. The lateral geniculate group is a known relay in the visual system, receiving afferents from the optic tract and projecting to the visual cortices via the optic radiation[45]. In keeping with this, we found dense projections in this region to the primary visual areas and temporal cortex. In contrast, the medial geniculate region is the primary relay for all ascending auditory information, projecting on to cortical auditory processing areas[46]. Correspondingly we found preferential projections to the primary auditory cortex, parietal cortex and brainstem in keeping with known the anatomy[46].

Thalamic nuclei transitional networks

We examined the degree of overlap in connectivity between regions of the topographic tractography gradients by sampling the voxels that contained the bottom, middle and top gradient quintiles (Fig. 6). Clear evidence was found for both segregated and overlapping networks in a graduated topographically arranged fashion in over 99% of all voxels across all subjects, with the mid-zone in most nuclei forming a broad, overlapping transition zone. Whilst we did find that some voxels broke this topographic arrangement (i.e. overlapping tracts between the top and bottom quintiles only), these were a minority representing 0.56% of all voxels and are unlikely to be significant. The transition zone in the geniculate group was much smaller, which is likely to reflect that this structure could be separated into medial and lateral components. Interestingly, the MD group also

displayed a similar, relatively abrupt transition zone suggesting that the anteriomedial and posteriolateral components of this nucleus separate into distinct sub-structures[35].

Thalamic nuclei reproducibility and overlap

To demonstrate the stability and reproducibility of the technique, segmentations are shown for nine subjects in Fig. 7 and Fig 8. Additionally, each of the segmentations for all subjects were warped to the group average space and used to create thalamic nuclei overlap maps. These show that despite inter-individual variability, high degree of overlap for the majority of the nuclei in affine registered (Supplementary Fig. 3) and warped group average space (Fig. 7).

To explore this further we used the thalamic nuclei overlap maps to calculate the threshold-overlap ratio, defined as the sum of all voxels binarised at a set threshold between zero and one, divided by the sum of all binarised voxels greater than zero. These threshold-overlap ratios were plotted across a range of segmentation thresholds for our data and the Oxford thalamic connectivity atlas[18] (Fig. 8). These confirmed the most stable segmentations with the highest degree of overlap and least inter-individual variation were the VP, VL, GEN and pANT groups. The lowest levels of overlap were observed in the dorso-medial aspect of the thalamus with overlap between voxels that were classified as the posterior part of VA or IL. This may reflect difficulties in tracking from regions with low anisotropy, causing greater uncertainty regarding tissue classification. Despite this the remainders of the clusters were extremely stable and reproducible, correspond well to the *ex vivo* data[3,50] (Supplementary Fig. 2) and displayed significantly higher overlap in group average space compared to the Oxford thalamic connectivity atlas (Fig. 8).

DISCUSSION

Here we demonstrate a technique for reliably delineating nine thalamic nuclei at an individual subject level by quantifying the white matter distributions computed using probabilistic tractography. Using an *a priori* free approach, we show that our *in vivo*

bottom-up clustering of white matter distribution properties produces a similar parcellation to that achieved by *ex vivo* cellular cytoarchitectual properties[1], and that these segmentations are highly reproducible across a population of 40 healthy individuals. Furthermore we define the pattern of whole brain connectivity for each thalamic nucleus, demonstrating a good correspondence to the animal literature[8,35,44-46]. We show the topographic transition gradients in whole-brain connectivity within each thalamic nucleus, and demonstrate a topographic arrangement of overlapping and non-overlapping projections. Due to the established principle of reciprocity between thalamocortical and corticothalamic projections[5], our observations provide objective MRI evidence to suggest that *spiral loops*[1], an arrangement of closed reciprocal and open non-reciprocal projections allowing information to flow between functionally distinct networks, may be present within each of our thalamic nuclei groups. Whilst the correspondence between tractography and tract tracing has been shown to be good at post mortem, with tractography capable of identifying >70% of all tracts provided attention is paid to the initial settings[55], this evidence should still be interpreted with caution due to known limitations associated with tractography. This includes limited number of fiber directions, inability to resolve fiber polarity, skew towards tracking dominant fiber systems and decreasing accuracy with long-range connections. Further work using *ex vivo* tract tracing techniques will be required to verify this.

Our segmentation technique was developed based upon several simple observations derived from the histological work into cytoarchitectual region delineation[19]. Specifically, by shifting the focus from "*patterns of connectivity*" to quantifying the intrinsic properties of white matter spatial distributions derived via probabilistic tractography, we avoided many of the assumptions and criticisms that have emerged through previous approaches including imposing *a priori* assumptions on the functional subdivision of the cortex[13-15] or the thalamus; down-sampling, thresholding, transforming the probabilistic tractography data[12,14]; or imposing potentially artificial hard-boundaries between clusters[47]. In doing so the intrinsic architectural properties of the thalamus, as quantified using probabilistic tractography, defines the internal structure using a bottom-up technique at an individual subject level. Of particular note is the similarity between

our results and those derived from cellular cytoarchitectual properties[1]. Despite operating at fundamentally different length scales, these separate imaging modalities converge upon a common architectural structure.

The internal topographic structure of the thalamic nuclei is complex; this has been further confounded by the many conflicting subdivisions and nomenclature systems that have emerged over time[4]. In part, these are a reflection of the fact that multiple overlapping maps can be defined within the same territory depending on the method used to delineate them. For example within the sensory VP nuclear group, multiple complete somatotopic representations of the entire body aligned along a curved superior-inferior axis can be defined based upon incoming sensory afferents. Each of these is composed of distinct spatial territories that project to and from a wide range of overlapping targets within the cortex, brainstem, cerebellum and spinal cord[48]. These somatotopic maps can be further separated according to sensory modality (e.g. light touch, vibration), with repeating bands of slow- or rapidly- adapting neurons that can be clustered into high- or low- response thresholds[49]. These observations can be reconciled with our topographic connectivity gradients by considering the maps in terms of their structural organizational hierarchy. Tractography cannot distinguish the polarity of the connections[13], therefore the topographic maps defined represent the sum total of the afferent and efferent fiber projection probabilities arising from a single voxel to the rest of the brain, and as such could be considered high-level maps. By thresholding these transitions, it is not only possible to select distinct zones with characteristic networks, but also further characterize the topographic organization within these narrow segments, that represent sub-levels of internal structure.

There are limitations with this current approach. First, we identify nine out of a proposed 30 thalamic nuclei[1]. Furthermore two of our groups encompass several nuclear groups. However, we have shown that each of our nuclei forms a topographic transition gradient between distinct cortical networks. These graduated transitions have also been observed between *ex vivo* nuclei, for example the divisions of the VL nucleus[1]. Consequently the actual number of subdivisions captured by this technique may well be closer to *ex vivo*

models. It is clear from the connectivity gradients that the thalamic nuclei presented here could be parcellated into further distinct regions. However, we opted against this in favor of objectively defining unique nuclei based on the feature maps, and identifying the topographic transitions in connectivity profiles within these regions. This avoids imposing artificial hard boundaries that have led to much misinterpretation and criticism in the past[47], representing the tractography data in a more biophysically realistic form and This also avoids the inherent difficulties in cluster number selection and implicitly allows functionally distinct regions of the nuclei to be easily defined. Whilst there is a risk that the depth of the seed voxel within the thalamus may cause a bias in the tractography gradients due to the greater number of voxels with higher uncertainty they must pass through, the average FA in the HCP data for the thalamus is reasonably constant (between 0.2-0.3) and we do not observe any gradients orientated to the depth from the white matter surface that would be more suggestive of this bias. Despite this, we cannot completely exclude seed depth as a contributory element to the gradients observed in this work. Whilst the Euclidean distance metric was used for this segmentation technique, it is also acknowledged that there are several other distance metrics that may be better suited to these datasets. However, our initial attempt in this work was to replicate the successful *ex vivo* methodologies employed in mapping cytoarchitectual regions. Future work will seek to optimize and build upon this approach, including assessing alternative measures of distance between tractography distributions. Furthermore, the thalamic segmentations were derived from a unimodal technique, which may contribute to some of the variability observed. Combining this with other imaging modalities, such as quantitative MRI or resting state fMRI, may provide opportunities to improve the segmentations still further. Whilst we have used high-resolution diffusion data from the Human Connectome Project, the tissue priors that were created can now be used with any probabilistic tractography dataset, after computation of the feature maps, and therefore has broad applicability. Finally, whilst a ground truth is not available for our study population we have demonstrated good correspondence to the histology (Fig. 8; Supplementary Fig. 2) and highlighted differences where they occur. Nevertheless, future datasets combining *in vivo* scanning and *ex vivo* histology will enable better understanding between MR defined features and underlying tissue microstructure.

Our segmentation technique provides a method to more accurately define thalamic nuclei at an individual subject level. A key application for this is to provide better alignment of thalamic nuclei in a group average space, potentially allowing thalamic function to be more precisely investigated using fMRI. Additionally, due to the bottom-up nature of these techniques, the normal variability in thalamic nuclei can be investigated, and the question whether distinct anatomical modes exist can be explored utilizing methods such as multi-atlas segmentation[65]. Even in the absence of tractography data, our ROIs had a high degree of 100% overlap at a group average level and will be made available through the Neuroimaging Informatics Tools and Resources Clearinghouse (NITRC). Additionally, there are translational motivations to this work. The thalamus is affected by a broad range of conditions including schizophrenia[56], Parkinson's disease[57], and Alzheimer's disease[58], and this approach could be used to better characterize the relationship between functional morbidity and thalamic pathology *in vivo*. Finally, in functional neurosurgery, deep brain stimulation is used to target specific thalamic nuclei in the treatment of certain conditions, such as the motor portion of VL in tremor disorders or the anterior nucleus in epilepsy, and therefore this technique could be used to improve surgical accuracy and help discover novel targets for other diseases that are modulated by the thalamus.

CONCLUSION:

In conclusion, we have demonstrated a technique to better delineate and align individual thalamic nuclei *in vivo*. This improves the quantification of inter-individual variability in these structures and allows homologous nuclei to be more accurately aligned, providing a broad basis for applications in functional and anatomical MRI research. It can be used both to study the normal functional properties of these regions, many of which still remain poorly understood, and also enable the subcortical progression of neurodegenerative diseases to be better characterized. Finally, there is potential for this technique to be applied to functional neurosurgery, where the specific thalamic nuclei are targeted using deep brain stimulation in the treatment of a variety of conditions including tremor, epilepsy and chronic pain.

Acknowledgements

CL is supported by The Academy of Medical Sciences Clinical Lecturer Start-Up Grant. Data were provided [in part] by the Human Connectome Project, WU-Minn Consortium (Principal Investigators: David Van Essen and Kamil Ugurbil; 1U54MH091657) funded by the 16 NIH Institutes and Centers that support the NIH Blueprint for Neuroscience Research; and by the McDonnell Center for Systems Neuroscience at Washington University.

REFERENCES

1.Haber, S. N. The primate basal ganglia: parallel and integrative networks. *J Chem Neuroanat* **26,** 317-30 (2003).

2.Llinás, R., Ribary, U., Jeanmonod, D., Cancro, R., Kronberg, E., Schulman, J., Zonenshayn, M., Magnin, M., Morel, A. and Siegmund, M. Thalamocortical dysrhythmia I. Functional and imaging aspects. *Thalamus & Related Systems* **1,** 237-244 (2001).

3.Morel, A. *Stereotactic atlas of the human thalamus and basal ganglia. Stereotactic atlas of the human thalamus and basal ganglia* (Informa Healthcare: 2007).

4.Percheron, G., Francois, C., Talbi, B., Yelnik, J. and Fenelon, G. The primate motor thalamus. *Brain research reviews* **22,** 93-181 (1996).

5.Jones, E. G. The thalamus. *The thalamus* (1985).at <http://dx.doi.org/10.1007/978-1-4615-1749-8>

6.Braak, H., Tredici, K. D., Rüb, U., de Vos, R. A., Jansen Steur, E. N. and Braak, E. Staging of brain pathology related to sporadic Parkinsons disease. *Neurobiology of aging* **24,** 197-211 (2003).

7.Braak, H. and Braak, E. Neuropathological stageing of Alzheimer-related changes. *Acta Neuropathol* **82,** 239-59 (1991).

8.Child and , B. E. Anterior nucleus of the thalamus Functional organization and clinical implications. *Neurology* **81,** 1869-1876 (2013).

9.Callaghan, P. T. *Principles of nuclear magnetic resonance microscopy. Principles of nuclear magnetic resonance microscopy* (Oxford University Press: 1993).

10.Behrens, T. E., Woolrich, M. W., Jenkinson, M., Johansen-Berg, H., Nunes, R. G., Clare, S., Matthews, P. M., Brady, J. M. and Smith, S. M. Characterization and propagation of uncertainty in diffusion-weighted MR imaging. *Magn Reson Med* **50,** 1077-88 (2003).doi:10.1002/mrm.10609

11.Dyrby, T. B., Søgaard, L. V., Parker, G. J., Alexander, D. C., Lind, N. M., Baaré, W. F. C., Hay-Schmidt, A., Eriksen, N., Pakkenberg, B. and Paulson, O. B. Validation of in vitro probabilistic tractography. *Neuroimage* **37,** 1267-1277 (2007).doi:10.1016/j.neuroimage.2007.06.022

12.Lambert, C., Zrinzo, L., Nagy, Z., Lutti, A., Hariz, M., Foltynie, T., Draganski, B., Ashburner, J. and Frackowiak, R. Confirmation of functional zones within the human subthalamic nucleus: patterns of connectivity and sub-parcellation using diffusion weighted imaging. *Neuroimage* **60,** 83-94 (2012).doi:10.1016/j.neuroimage.2011.11.082

13.Behrens, T. E., Johansen-Berg, H., Woolrich, M. W., Smith, S. M., Wheeler-Kingshott, C. A., Boulby, P. A., Barker, G. J., Sillery, E. L., Sheehan, K., Ciccarelli, O., Thompson, A. J., Brady, J. M. and Matthews, P. M. Non-invasive mapping of connections between human thalamus and cortex using diffusion imaging. *Nat Neurosci* **6,** 750-7 (2003).doi:10.1038/nn1075

14.Draganski, B., Kherif, F., Klöppel, S., Cook, P. A., Alexander, D. C., Parker, G. J., Deichmann, R., Ashburner, J. and Frackowiak, R. S. Evidence for segregated and integrative connectivity patterns in the human Basal Ganglia. *J Neurosci* **28,** 7143-52 (2008).doi:10.1523/JNEUROSCI.1486-08.2008

15.Broser, P., Vargha-Khadem, F. and Clark, C. A. Robust subdivision of the thalamus in children based on probability distribution functions calculated from probabilistic tractography. *Neuroimage* **57,** 403-15 (2011).doi:10.1016/j.neuroimage.2011.04.054

16.Kumar, V., Mang, S. and Grodd, W. Direct diffusion-based parcellation of the human thalamus. *Brain Struct Funct* (2014).doi:10.1007/s00429-014-0748-2

17.Amunts, K., Malikovic, A., Mohlberg, H., Schormann, T. and Zilles, K. Brodmann's areas 17 and 18 brought into stereotaxic space-where and how variable? *Neuroimage* **11,** 66-84 (2000).doi:10.1006/nimg.1999.0516

18.Johansen-Berg, H., Behrens, T. E., Sillery, E., Ciccarelli, O., Thompson, A. J., Smith, S. M. and Matthews, P. M. Functional-anatomical validation and individual variation of diffusion tractography-based segmentation of the human thalamus. *Cereb Cortex* **15,** 31-9 (2005).doi:10.1093/cercor/bhh105

19.Schleicher, A., Amunts, K., Geyer, S., Morosan, P. and Zilles, K. Observer-independent method for microstructural parcellation of cerebral cortex: A quantitative approach to cytoarchitectonics. *Neuroimage* **9,** 165-77 (1999).doi:10.1006/nimg.1998.0385

20.Glasser, M. F., Sotiropoulos, S. N., Wilson, J. A., Coalson, T. S., Fischl, B., Andersson, J. L., Xu, J., Jbabdi, S., Webster, M., Polimeni, J. R., DC, V. E. and Jenkinson, M. The Minimal Preprocessing Pipelines for the Human Connectome Project. *NeuroImage* **80,** 105-124 (2013).doi:10.1016/j.neuroimage.2013.04.127

21.Hernández, M., Guerrero, G. D., Cecilia, J. M., García, J. M., Inuggi, A., Jbabdi, S., Behrens, T. E. and Sotiropoulos, S. N. Accelerating fiber orientation estimation from diffusion weighted magnetic resonance imaging using GPUs. *PLoS One* **8,** e61892 (2013).doi:10.1371/journal.pone.0061892

22.Ashburner, J. and Friston, K. J. Unified segmentation. *Neuroimage* **26,** 839-51 (2005).doi:10.1016/j.neuroimage.2005.02.018

23.Ashburner, J. and Friston, K. J. Diffeomorphic registration using geodesic shooting and Gauss-Newton optimisation. *Neuroimage* **55,** 954-67 (2011).doi:10.1016/j.neuroimage.2010.12.049

24.Yushkevich, P. A., Piven, J., Hazlett, H. C., Smith, R. G., Ho, S., Gee, J. C. and Gerig, G. User-guided 3D active contour segmentation of anatomical structures: significantly improved efficiency and reliability. *Neuroimage* **31,** 1116-28 (2006).doi:10.1016/j.neuroimage.2006.01.015

25.Lu, N., Wang, J., Wu, Q. H. and Yang, L. An improved motion detection method for real-time surveillance. *IAENG International Journal of Computer Science* **35,** 1-10 (2008).

26.Lambert, C., Lutti, A., Helms, G., Frackowiak, R. and Ashburner, J. Multiparametric brainstem segmentation using a modified multivariate mixture of Gaussians. *NeuroImage: Clinical* **2,** 684-694 (2013).doi:10.1016/j.nicl.2013.04.017

27.Cruce, J. A. An autoradiographic study of the projections of the mammillothalamic tract in the rat. *Brain Research* **85,** 211-219 (1975).doi:10.1016/0006-8993(75)90072-4

28.Mitchell, A. S., Dalrymple-Alford, J. C. and Christie, M. A. Spatial working memory and the brainstem cholinergic innervation to the anterior thalamus. *The Journal of neuroscience* **22,** 1922-1928 (2002).

29.Guandalini, P. The efferent connections to the thalamus and brainstem of the physiologically defined eye field in the rat medial frontal cortex. *Brain research bulletin* **54,** 175-186 (2001).

30.Kalil, K. Projections of the cerebellar and dorsal column nuclei upon the thalamus of the rhesus monkey. *Journal of Comparative Neurology* **195,** 25-50 (1981).

31.Schmahmann, J. D. and Pandya, D. N. Anatomical investigation of projections from thalamus to posterior parietal cortex in the rhesus monkey: a WGA-HRP and fluorescent tracer study. *Journal of Comparative Neurology* **295,** 299-326 (1990).

32.Schmahmann, J. D. Vascular syndromes of the thalamus. *Stroke* **34,** 2264-78 (2003).doi:10.1161/01.STR.0000087786.38997.9E

33.Rouiller, E. M., Tanne, J., Moret, V. and Boussaoud, D. Origin of thalamic inputs to the primary, premotor, and supplementary motor cortical areas and to area 46 in macaque monkeys: a multiple retrograde tracing study. *Journal of Comparative Neurology* **409,** 131-152 (1999).

34.Watanabe, Y. and Funahashi, S. Thalamic mediodorsal nucleus and working memory. *Neuroscience & Biobehavioral Reviews* **36,** 134-142 (2012).doi:10.1016/j.neubiorev.2011.05.003

35.Mitchell, A. S. and Chakraborty, S. What does the mediodorsal thalamus do? *Front Syst Neurosci* **7,** 37 (2013).doi:10.3389/fnsys.2013.00037

36.Klein, J. C., Rushworth, M. F., Behrens, T. E., Mackay, C. E., de Crespigny, A. J., D'Arceuil, H. and Johansen-Berg, H. Topography of connections between human prefrontal cortex and mediodorsal thalamus studied with diffusion tractography. *Neuroimage* **51,** 555-564 (2010).

37.Pare, D., Smith, Y., Parent, A. and Steriade, M. Projections of brainstem core cholinergic and non-cholinergic neurons of cat to intralaminar and reticular thalamic nuclei. *Neuroscience* **25,** 69-86 (1988).

38.Saalmann, Y. B. Intralaminar and medial thalamic influence on cortical synchrony, information transmission and cognition. *Front Syst Neurosci* **8,** 83 (2014).doi:10.3389/fnsys.2014.00083

39.Scheibel, M. E. and Scheibel, A. B. The organization of the ventral anterior nucleus of the thalamus. A Golgi study. *Brain Research* **1,** 250-268 (1966).

40.Carmel, P. W. Efferent projections of the ventral anterior nucleus of the thalamus in the monkey. *American Journal of Anatomy* **128,** 159-183 (1970).doi:10.1002/aja.1001280204

41.Tekin, S. and Cummings, J. L. Frontal--subcortical neuronal circuits and clinical neuropsychiatry: an update. *Journal of psychosomatic research* **53,** 647-654 (2002).

42.Barbas, H., García-Cabezas, M. Á. and Zikopoulos, B. Frontal-thalamic circuits associated with language. *Brain Lang* **126,** 49-61 (2013).doi:10.1016/j.bandl.2012.10.001

43.Schell, G. R. and Strick, P. L. The origin of thalamic inputs to the arcuate premotor and supplementary motor areas. *The Journal of neuroscience* **4,** 539-560 (1984).

44.Gopathy Purushothaman, R. M. K. L. V. A. C. Gating and control of primary visual cortex by pulvinar. *Nature neuroscience* **15,** 905 (2012).doi:10.1038/nn.3106

45.Bürgel, U., Schormann, T., Schleicher, A. and Zilles, K. Mapping of histologically identified long fiber tracts in human cerebral hemispheres to the MRI volume of a reference brain: position and spatial variability of the optic radiation. *Neuroimage* **10,** 489-499 (1999).

46.Winer, J. A. *The Functional Architecture of the Medial Geniculate Body and the Primary Auditory Cortex. The Mammalian Auditory Pathway: Neuroanatomy* 222-409 (Springer New York: 1992).doi:10.1007/978-1-4612-4416-5_6

47.Lambert, C., Zrinzo, L., Nagy, Z., Lutti, A., Hariz, M., Foltynie, T., Draganski, B., Ashburner, J. and Frackowiak, R. Do we need to revise the tripartite subdivision hypothesis of the human subthalamic nucleus (STN)? Response to Alkemade and Forstmann. *NeuroImage* **110,** 1-2 (2015).doi:10.1016/j.neuroimage.2015.01.038

48.Dykes, R. W., Landry, P., Hicks, T. P., Diadori, P. and Metherate, R. Specificity of connections in the ventroposterior nuclei of the thalamus. *Progress in neurobiology* **30,** 87-103 (1988).

49.Kaas, J. H., Nelson, R. J., Sur, M., Dykes, R. W. and Merzenich, M. M. The somatotopic organization of the ventroposterior thalamus of the squirrel monkey, Saimiri sciureus. *J Comp Neurol* **226,** 111-40 (1984).doi:10.1002/cne.902260109

50. Amunts, K., Lepage, C., Borgeat, L., Mohlberg, H., Dickscheid, T., Rousseau, M.É., Bludau, S., Bazin, P.L., Lewis, L.B., Oros-Peusquens, A.M. and Shah, N.J. BigBrain: an ultrahigh-resolution 3D human brain model. *Science* **340** (6139): 1472–1475 (2013).

51. Haber, S.N., Fudge, J.L., McFarland, N.R., 2000. Striatonigrostriatal pathways in primates form an ascending spiral from the shell to the dorsolateral striatum. J. Neurosci. 20 (6), 2369-2382.

52. Mang, S.C., Busza, A., Reiterer, S. and Grodd, W., 2012. Thalamus segmentation based on the local diffusion direction: a group study. *Magnetic resonance in medicine*, *67*(1), pp.118-126.

53. Stough, J.V., Glaister, J., Ye, C., Ying, S.H., Prince, J.L. and Carass, A., 2014. Automatic method for thalamus parcellation using multi-modal feature classification. In Medical Image Computing and Computer-Assisted Intervention–MICCAI 2014 (pp. 169-176). Springer International Publishing.

54. Andersson JLR, Jenkinson M, Smith S (2010) Non-linear registration, aka spatial normalisation. FMRIB technical report TR07JA2

55. Krauth, A., Blanc, R., Poveda, A., Jeanmonod, D., Morel, A. and Székely, G., 2010. A mean three-dimensional atlas of the human thalamus: generation from multiple histological data. *Neuroimage*, *49*(3), pp.2053-2062.

56. Byne, W., Buchsbaum, M.S., Mattiace, L.A., Hazlett, E.A., Kemether, E., Elhakem, S.L., Purohit, D.P., Haroutunian, V. and Jones, L., 2002. Postmortem assessment of thalamic nuclear volumes in subjects with schizophrenia. *American Journal of Psychiatry*.

57. Braak, H., Del Tredici, K., Rüb, U., de Vos, R.A., Steur, E.N.J. and Braak, E., 2003. Staging of brain pathology related to sporadic Parkinson's disease. *Neurobiology of aging*, *24*(2), pp.197-211.

58. Braak, H. and Braak, E., 1991. Neuropathological stageing of Alzheimer-related changes. *Acta neuropathologica*, *82*(4), pp.239-259.

59. Ruschel, M., Knösche, T.R., Friederici, A.D., Turner, R., Geyer, S., Anwander, A., 2014. Connectivity architecture and subdivision of the human inferior parietal cortex revealed by diffusion MRI. Cereb. Cortex 24 (9), 2436-2448.
60. Caspers, J., Zilles, K., Amunts, K., Laird, A.R., Fox, P.T., Eickhoff, S.B., 2014. Functional char-acterization and differential coactivation patterns of two cytoarchitectonic visual areas on the human posterior fusiform gyrus. Hum. Brain Mapp. 35 (6), 2754-2767.
61. O'Donnell, L.J., Golby, A.J., Westin, C.F., 2013. Fiber clustering versus the parcellation-based connectome. NeuroImage 80, 283-289.
62. Gan, G., Ma, C., Wu, J., 2007. Data Clustering: Theory, Algorithms, and Applications Vol. 20. Siam.
63. Jain, A.K., 2010. Data clustering: 50 years beyond K-means. Pattern Recogn. Lett. 31 (8), 651-666.
64. Accolla, E.A., Dukart, J., Helms, G., Weiskopf, N., Kherif, F., Lutti, A., Chowdhury, R., Hetzer, S., Haynes, J.R., Kühn, A.A., Draganski, B., 2014. Brain tissue properties differentiate between motor and limbic basal ganglia circuits. Hum. Brain Mapp. 35 (10), 5083-5092.
65. Aljabar, P., Heckemann, R. A., Hammers, A., Hajnal, J. V., & Rueckert, D. (2009). Multi-atlas based segmentation of brain images: atlas selection and its effect on accuracy. *Neuroimage*, *46*(3), 726-738.

SUPPLEMENTARY MATERIAL

Supplementary Figure 1: Thalamic nuclei – Renderings Three-dimensional renderings of the group average overlays for the nine thalamic nuclei. Labeling a-i as shown in Fig.4 legend**.**

Supplementary Figure 2: Thalamic nuclei – Overlap with Morel's histological atlas: Percentage overlap with the mean three-dimensional atlas of the human thalamus (licensed from University of Zurich and ETH Zurich; © University of Zurich and ETH

Zurich , Axel Krauth, Rémi Blanc, Alejandra Poveda, Daniel Jeanmonod, Anne Morel, Gábor Székely; Krauth et al., 2010). The overlap represents the percentage volume of each atlas thalamic nucleus occupied by the corresponding tractography thalamic segmentation with the highest probability of being located within that region.

Supplementary Figure 3: Supplementary Figure 3: Thalamic nuclei – Aligned using affine transformation (12 degrees of freedom) average overlap

Supplementary Figure 4: Cortical connectivity rose plot legend

Supplementary Figure 5: Sub-cortical connectivity rose plot legend

Supplementary Table 1: Thalamic nuclei – Overlap with histological atlas

Supplementary Table 2: Average thalamic nuclei normalized connectivity strength expressed as a percentage across all values for each individual Freesurfer ROI**.**

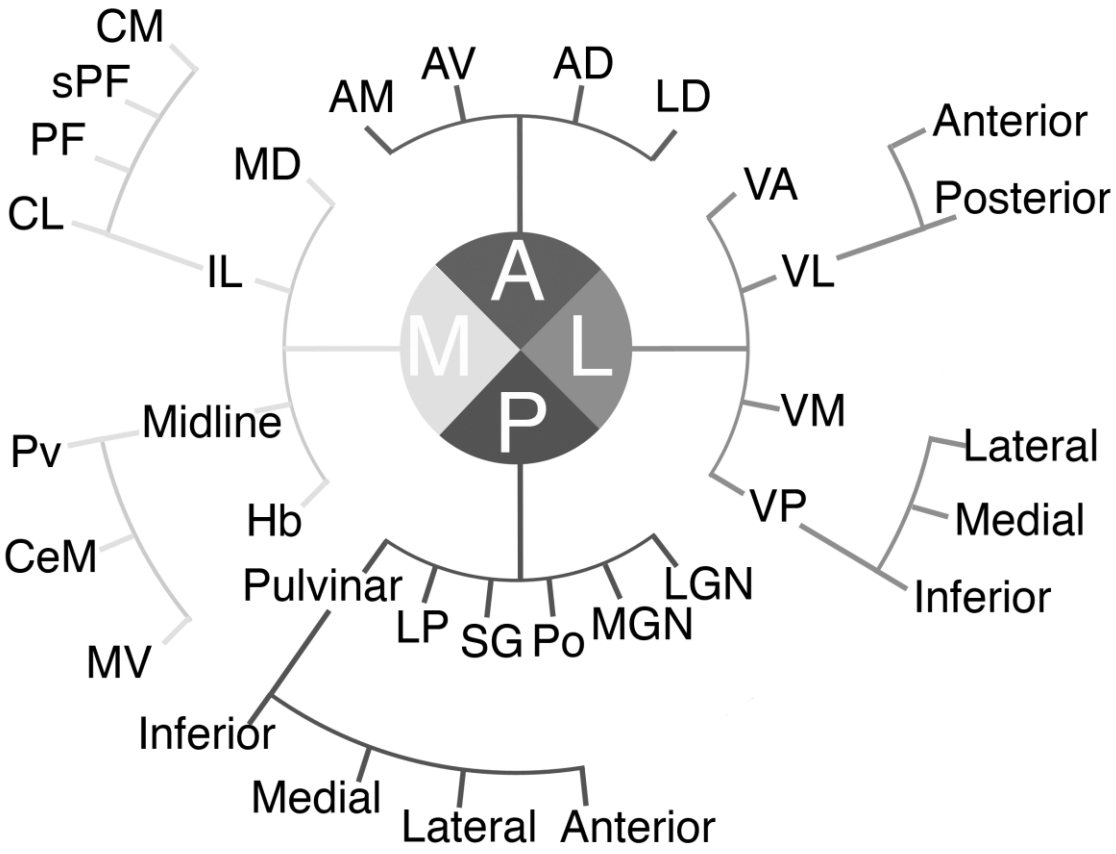

Figure 1: Morel's subdivision of the main thalamic groups. Abbreviations: A - Anterior Group: AM - Anteromedial, AV - Anteroventral, AD - Anterodorsal, LD - Lateral Dorsal. L - Lateral Group: VA - Ventral Anterior, VM - Ventral Medial, VL - Ventral Lateral, VP - Ventral Posterior. P - Posterior Group: MGN - Medial geniculate nucleus, LGN - Lateral geniculate nucleus, Po - Posterior nucleus, SG - Supragenicular/limitans, LP - Lateral Posterior. M - Medial Group: MD - Mediodorsal, CeM - Central Medial, Pv - Paraventricular, MV - Medioventral, Hb - Habenula, IL - Intralaminar, CL - Central Lateral, PF - Parafascicular, sPF - Subparafascicular, CM - Central Median. Note reticular not shown.

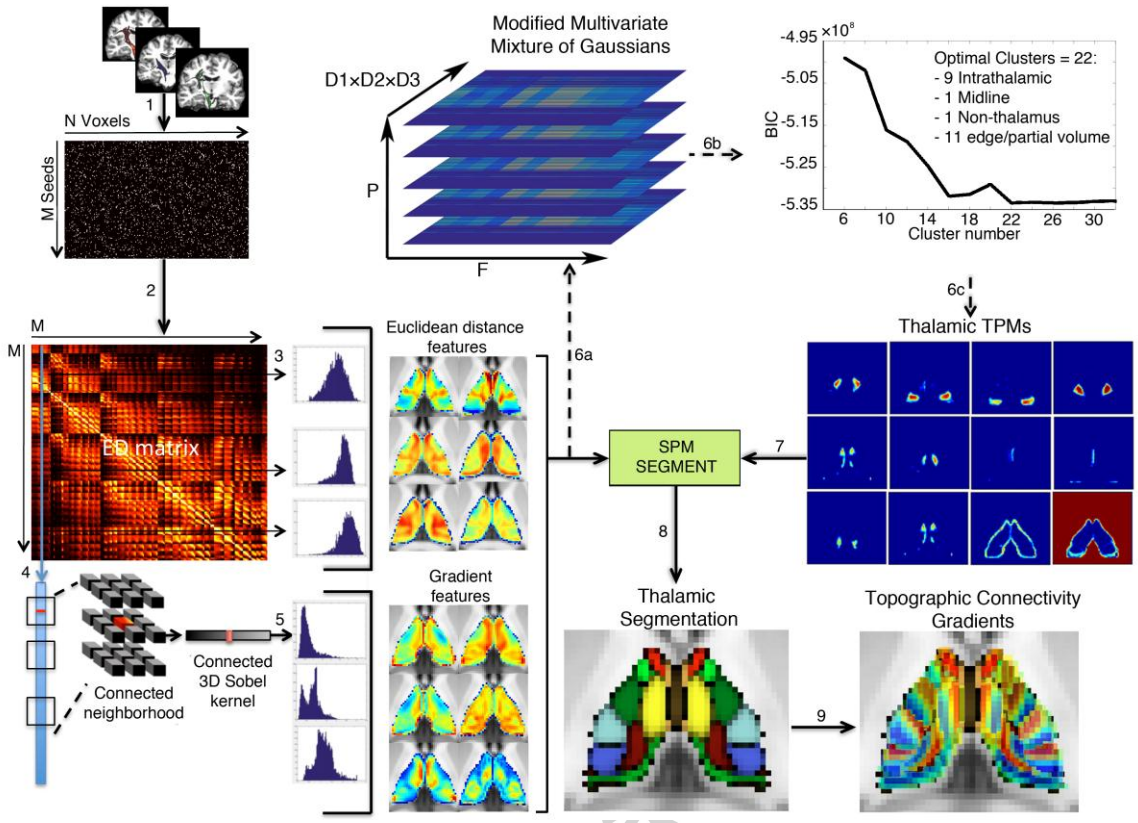

Figure 2: Thalamic Tractography Segmentation – Summary. Refer to the methods for a detailed breakdown of each step.

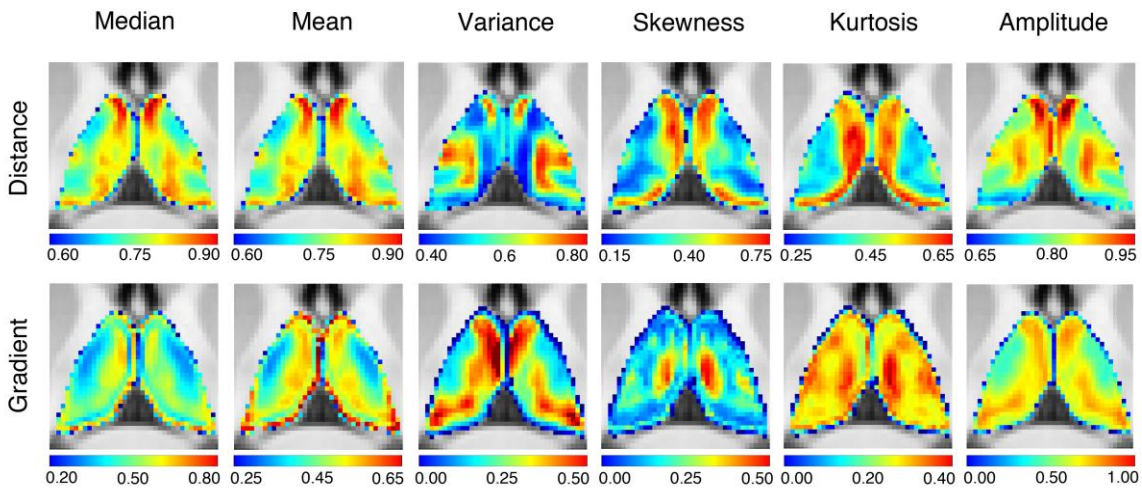

Figure 3: Feature maps. Group average, normalized feature maps derived from the Euclidean distance matrix. Six from the ED vectors, and six from the three-dimensional gradients between local neighborhoods of ED vectors.

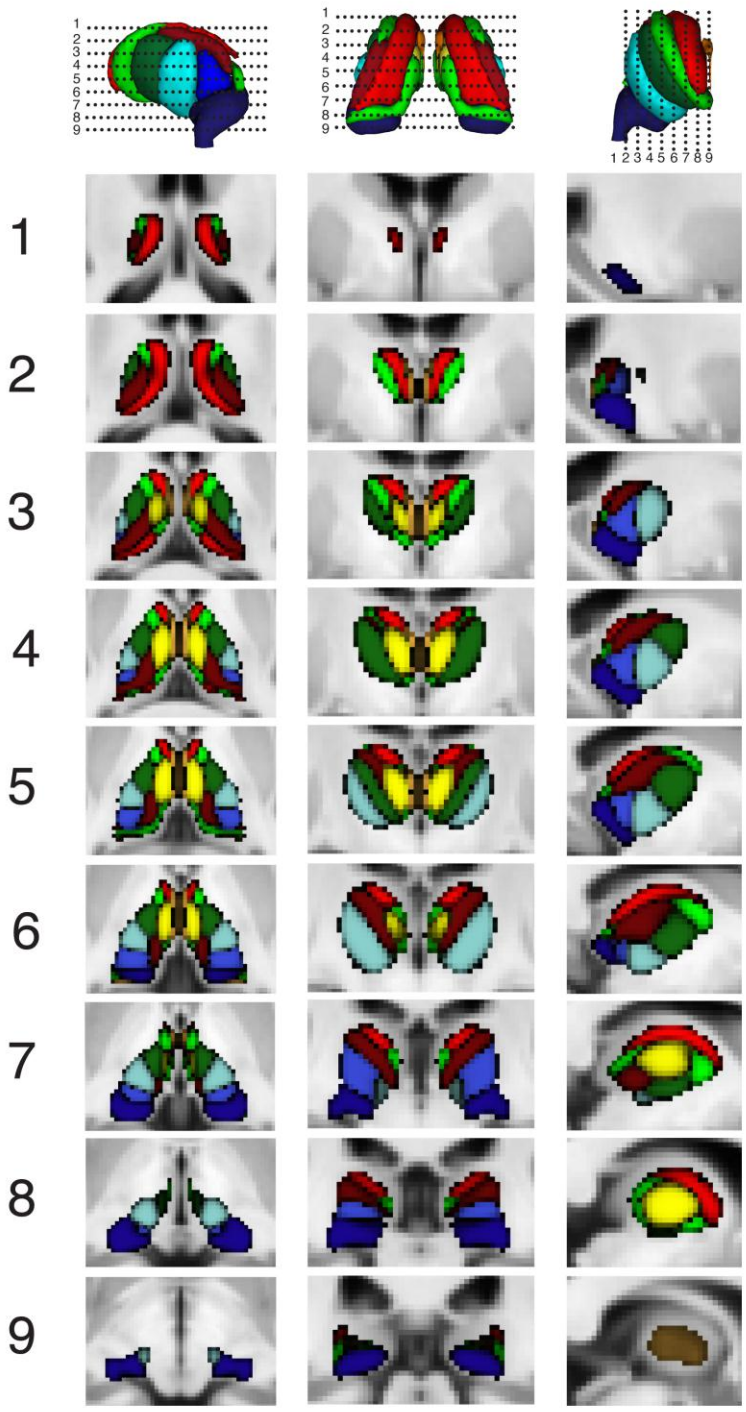

Figure 4: Thalamic nuclei – Segmentations. Group average overlays for the nine thalamic nuceli. Nuclei labeled according to closest aligning structure from the histological atlas[3] (Fig. 8): a. Anterior (ANT - red); b. Posterior Anterior (pANT - dark red); c. Mediodorsal (MD - yellow); d. Midline intralaminar (IL - orange); e. Ventroanterior (VA - light green); f. Ventrolateral (VL - dark green); g. Ventroposterior (VP - turquoise); h. Pulvinar (PUL); i. Geniculate (GEN - Dark Blue).

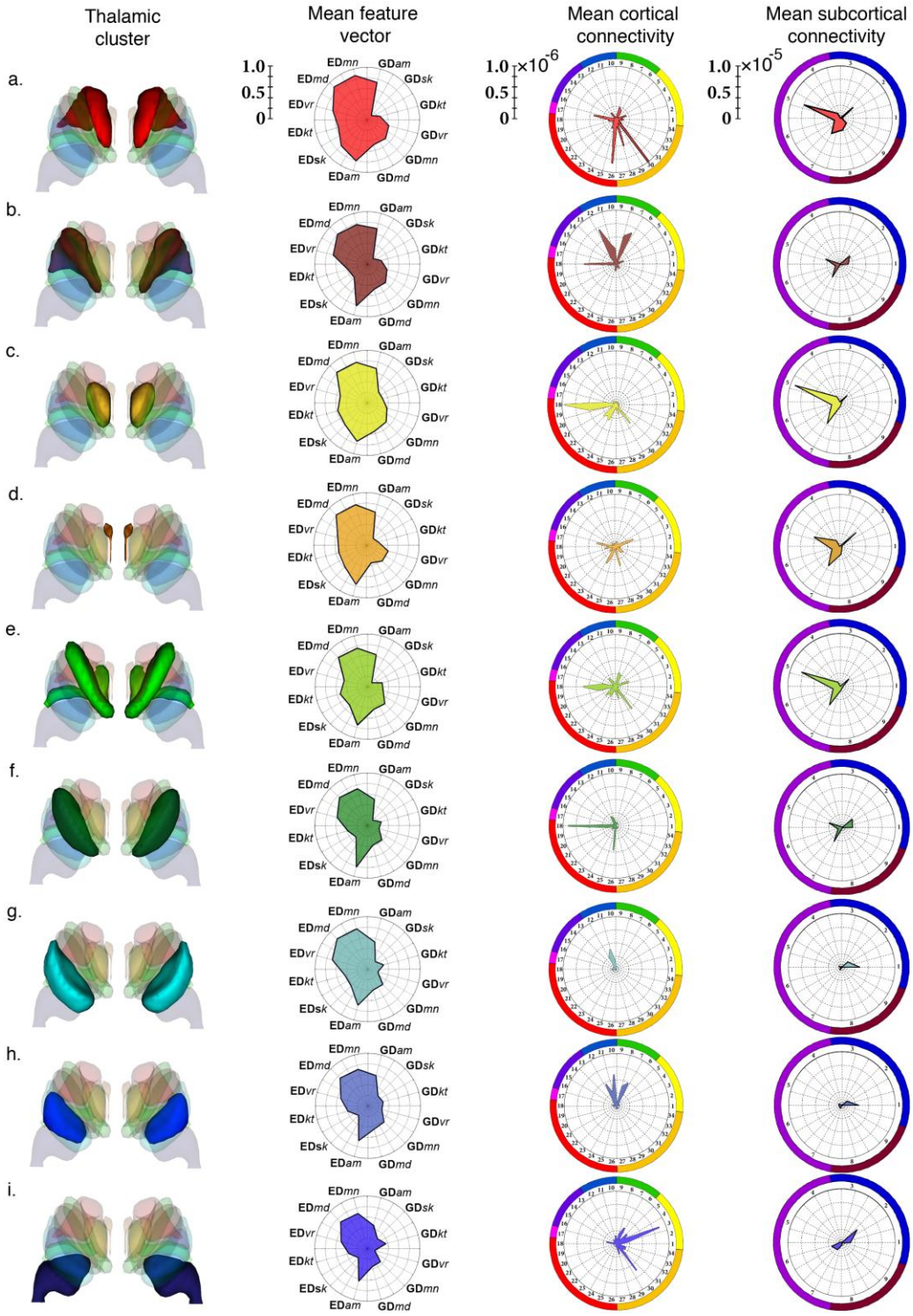

Figure 5: Thalamic nuclei – Properties. Group average properties showing the average feature map parameters, cortical and subcortical connectivity. Please refer to Supplementary Fig. 4 and 5 for annotated connectivity legends. Labeling a-i as summarised in Fig.4 legend**.**

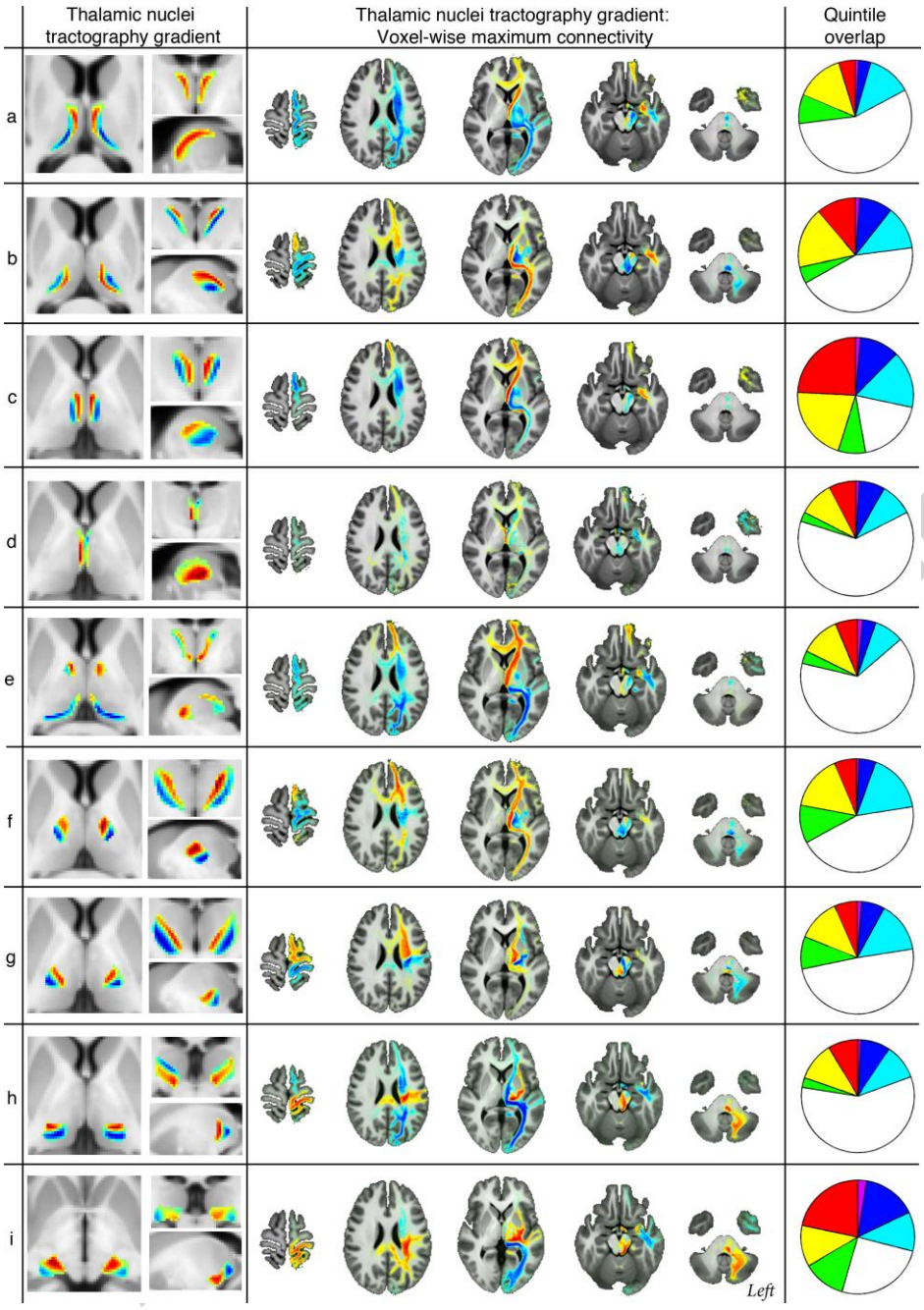

Figure 6: Thalamic nuclei – Connectivity Gradients. Transition gradients in the connectivity profiles for each thalamic nuclei. The axial brain slices show the tractography profile for each corresponding nucleus, and each voxel within the tract shows the gradient value of the seed with the strongest connectivity. The pie charts show the quintile overlaps (Blue: Low quintile only; Turquoise: Low-middle quintile overlap; Green: Middle quintile only; Yellow: Middle-high quintile overlap; White: All quintiles overlap; Red: High quintile only; Purple: High-low quintile overlap). This shows a topographically arranged graduated pattern of separated and overlapping tractography profiles.

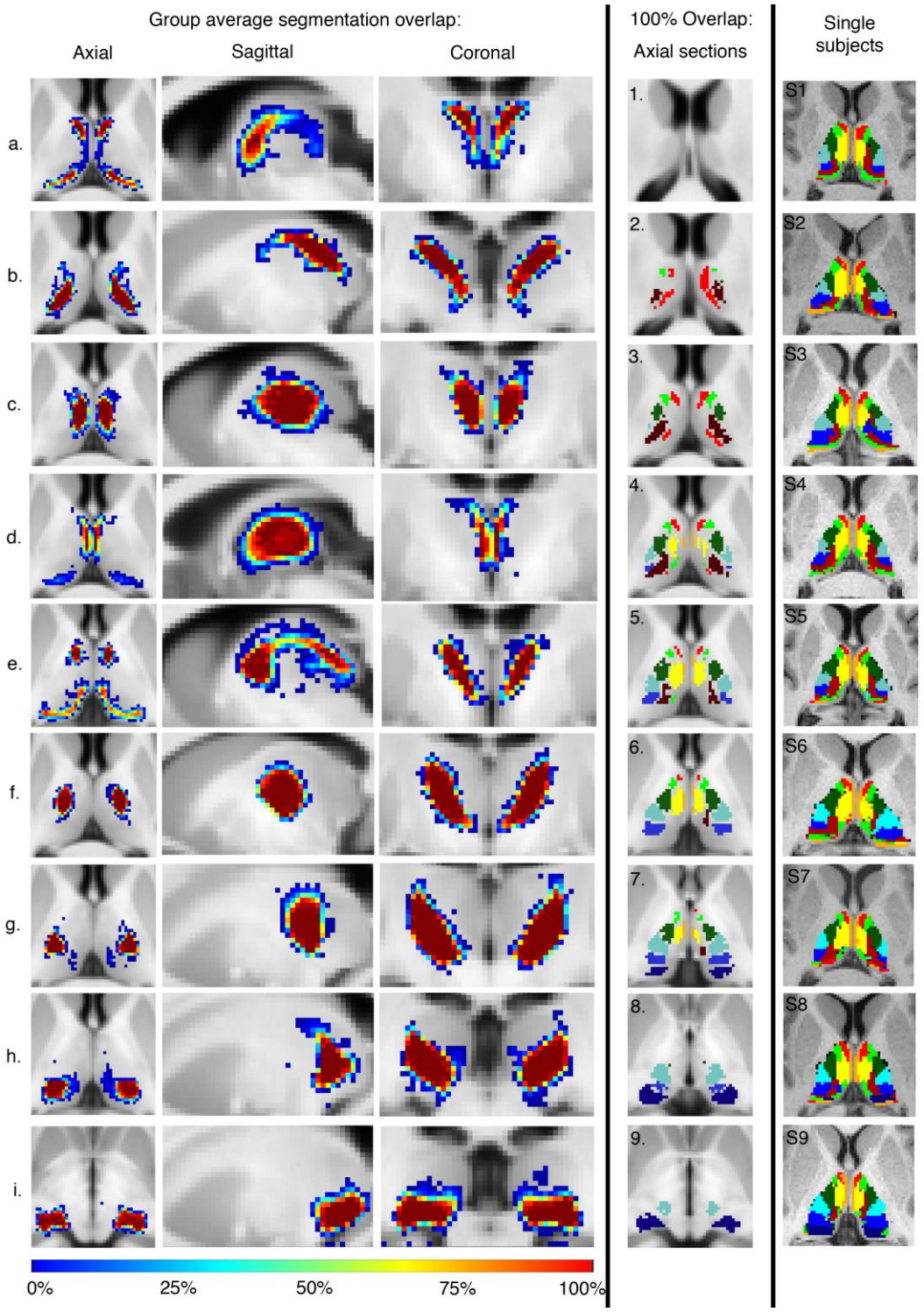

Figure 7: Thalamic nuclei – Group Average Variability. Group average for each thalamic segmentation shown on left, labeling a-i as summarised in Fig.4 legend. Middle column shows axial sections with all thalamic segmentations where the overlap was 100% (numbering corresponds to axial level shown in Fig. 3). Nine individual subject segmentations shown on the right.

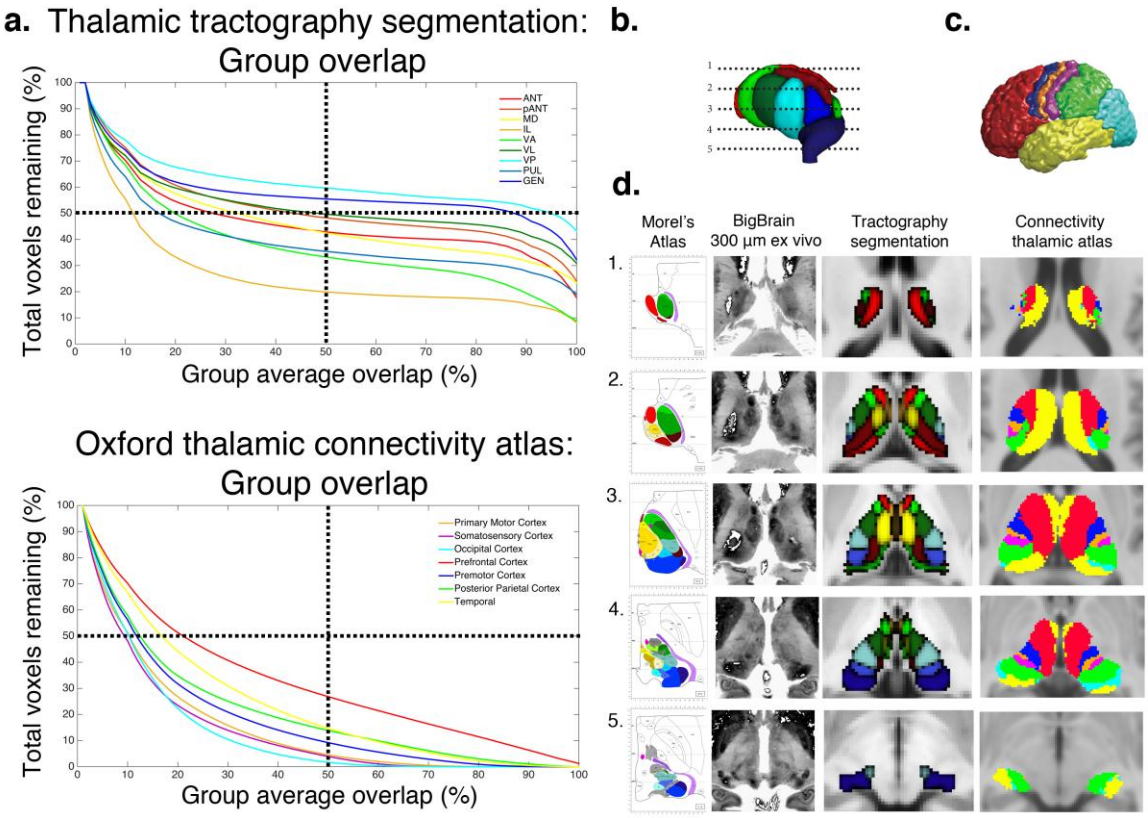

Figure 8: Group overlap and *ex vivo* comparison. a. Percentage overlap of each thalamic nucleus (ratio of total warped volume to volume at corresponding group average overlap threshold). b. Corresponding thalamic axial sections. c. Oxford thalamic connectivity atlas maximum connectivity regions: Red – Prefrontal cortex; Orange – Primary motor cortex; Mauve – Somatosensory cortex; Green – Posterior parietal cortex; Cyan – Occipital cortex; Yellow – Temporal cortex. d. Comparison of current method and Oxford thalamic connectivity atlas[13,18] against closest sections from Morel's Thalamic Atlas[3] and the Big Brain[50] 300µm histological sections.